Modeling of Frequency Security Constraints and Quantification of Frequency Control Reserve Capacities for Unit Commitment

Likai Liu, Zechun Hu, *Senior Member, IEEE*, Yilin Wen, *Student Member, IEEE*, and Yuxin Ma, *Student Member, IEEE*

***Abstract*—The high penetration of converter-based renewable energy sources has brought challenges to the power system frequency control. It is essential to consider the frequency security constraints and frequency control reserve requirements in unit commitment (UC). First, a novel extreme learning machine-based method is proposed to approximate the highly nonlinear frequency nadir constraint (FNC) by a set of linear constraints. Second, considering the variation of the frequency insecurity risk under the changing operational condition, we propose to optimize the primary frequency control (PFC) droop gains and reserve capacities in the UC model to provide diverse control efforts in different risk levels adaptively. Third, a secondary frequency control (SFC) reserve capacity quantification method is proposed by combining the Copula theory and distributionally robust optimization technique. The UC simulation is conducted on the IEEE 118-bus system to test the proposed optimal PFC droop gain strategy and SFC reserve capacity quantification method. Simulation results show that the proposed optimal PFC droop gain strategy is better than the traditional fixed PFC droop gain setting on economic efficiency and operational flexibility. Besides, the SFC reserve capacity calculated by the proposed method is more appropriate than the actual SFC reserve capacity in the historical operation.**

***Index Terms*—Unit commitment, frequency security constraints, frequency control reserve requirement, primary frequency control.**

NOMENCLATURE

Abbreviation

FNC	Frequency nadir constraint.
DSFR	Demand-side flexible resource.
FNCPD	Frequency nadir constrained power disturbance.
PFC	Primary frequency control.
RoCoF	Rate of change of frequency.
ELM	Extreme learning machine.
SFC	Secondary frequency control.
TG	Traditional generator.
UC	Unit commitment.

Indices & sets

n	Index of buses.
t	Index of dispatch periods.
$\mathcal{I}, \mathcal{J}$	Set of TGs and converter-based DSFRs.
$\mathcal{W}, \mathcal{S}$	Set of wind and solar power plants.
$\Im$	Set of power transmission lines.

Parameters

B	Susceptance of the transmission line.
C^{SU}	Start-up cost of generator.
$C_i^{\mathrm{Spin}}, C_i^{\mathrm{SFC}}$	Spinning and SFC reserve costs.
D, H	Normalized damping and inertia factors of the centralized frequency response model.
F^{Re}	High-pressure turbine fraction of the reheat steam turbine.
$\Delta f_{\max}^{\mathrm{Nadir/QSS}}$	Nadir/quasi-steady-state frequency deviation limit.
L	Power system load power.
$\bar{M}_i, \underline{M}_i$	Upper and lower limits of the PFC droop gain of frequency regulation resource i.
$P^{\max}, P^{\min}$	Maximum and minimum power outputs of TG.
P^{Fore}	Forecasted power output of a renewable generation resource.
P^{b}	Base operational point of DSFR.
$\Delta P, \Delta f$	Power imbalance and frequency deviation.
$r_{\mathrm{Req}}^{\mathrm{Op}+/-}$	Upward/downward operation reserve requirement.
$r_{\mathrm{Step}}^{\mathrm{SFC}}$	Step size of capacity when calculating SFC reserve requirement.
$r_{\min}^{\mathrm{SFC}}$	Minimum SFC reserve capacity in historical data.
$R^{\mathrm{g}}, R^{\mathrm{b}}$	Droop factors of TG and DSFR.
$RoCoF_{\max}$	Rate of change of frequency maximum limit.
$S^{\mathrm{g/b}}, S^{\mathrm{base}}$	Capacity of TG/DSFR and power base value.
$T^{\mathrm{Go}}, T^{\mathrm{Tu}}$	Governor and turbine time constant of TG.
$T^{\mathrm{ON}}, T^{\mathrm{OFF}}$	Minimum online and offline times of TG.
T^{Re}	Reheater time constant of TG.
T^{Co}	Converter time constant of DSFR.
V	Ramp rate of a generation resource.
W	Capacity of the transmission line.

Manuscript received 27 September 2022; revised 19 January 2023; accepted 26 February 2023. Date of publication 6 March 2023; date of current version 26 December 2023. This work was supported by the Key Research and Development Program of Inner Mongolia, China under Grant 2021ZD0039. *(Corresponding author: Zechun Hu.)*

The authors are with the Department of Electrical Engineering, Tsinghua University, Beijing 100084, China (e-mail: llk17@mails.tsinghua.edu.cn; zechhu@tsinghua.edu.cn; wen-yl20@mails.tsinghua.edu.cn).

Color versions of one or more figures in this article are available at https://doi.org/10.1109/TPWRS.2023.3252502.

Digital Object Identifier 10.1109/TPWRS.2023.3252502

$\phi^{\mathrm{g}}_{i,k}, \varphi^{\mathrm{g}}_{i,k}$	First-degree/constant term coefficient of the piecewise-linear generation cost function of generator i on the k^{th} segment.

Decision variables

P^{g}	Base operational point of TG.
$r^{\mathrm{Op}+/-}$	Upward/downward operation reserve capacity.
$r^{\mathrm{Spin}+/-}$	Upward/downward spinning reserve capacity.
$r^{\mathrm{PFC}+}, r^{\mathrm{PFC}-}$	Upward and downward PFC reserve capacities.
$r^{\mathrm{SFC}+}, r^{\mathrm{SFC}-}$	Upward and downward SFC reserve capacities.
x^{g}	Binary variable representing the ON/OFF status of TG.
x^{PFC}	Binary variable indicating whether a regulation resource participates in PFC.
y, z	Binary variables representing the start-up and shutdown processes of TG.
$K^{\mathrm{g}}, K^{\mathrm{b}}$	Droop gains of TG and DSFR.
θ	Voltage angle of the bus.

I. Introduction

CARBON neutral has become a consensus of most countries in the world. To achieve this ambitious goal, 33% and 25% of the total power generation should be provided by wind and solar by 2050 [1]. The high penetration of renewable generations will lower the system inertia level and intensify the power fluctuation, jeopardizing the frequency quality and increasing the risk of frequency instability [2], [3], [4]. Thus, it is essential to consider the frequency control in power system scheduling.

The results of unit commitment will determine the frequency response model and the largest power loss under N-1 contingency [5]. They both have significant influences on the power system frequency security. Thus, considering frequency security constraints in UC has been an active research direction recently [6].

The frequency security constraints require the RoCoF, quasi-steady-state frequency deviation, and frequency nadir within their limits [7], among which the FNC is highly nonlinear [8]. To preserve the linearity of the power system scheduling models, several methods have been proposed to simplify the FNC. The first kind of method assumes that the regulation resource changes its output with a constant ramp rate during the primary frequency control process [9], [10], which is not consistent with the droop control strategy adopted by the frequency regulation resources. The second type [11], [12], [13] utilizes the multistage approximation. In the first stage, the full-order frequency response model is simplified and reduced to a low-order model, and the nonlinear frequency nadir formulation is derived from this model. The second stage is to fit the frequency nadir expression through piecewise linearization. It has been proved in [14] that the accuracy of the second method is better than that of the first. However, the fitting error may be superposed and amplified in this multistage approximation method. The third type utilizes the machine learning technique to linearize the FNC. Lagos et al. utilized the optimal decision tree to fit the original FNC [15], but the decision-tree based method may identify the unsafe operation plan as a safe one, which has a large influence on the power system security. Zhang et al. used the deep neural network (DNN) to approximate the original FNC by a set of mixed integer linear constraints [16], [17]. By adding a margin to the obtained linear constraints, it is guaranteed that no unsafe operation plan will be identified as a safe one. However, the DNN-based FNC introduces a large number of additional integer variables (not the UC on/off variables), which increase the computational complexity of FNC approximation and the UC problem.

Another critical issue is the variable risk of frequency insecurity. The large-scale integration of renewable generations increases the variation ranges of key parameters in the frequency response model [18], [19], such as the inertial level, resulting in the varying risk of frequency insecurity. The droop gain decides the power regulation from PFC, which has prominent influences on the frequency security. Nevertheless, the droop gains of PFC resources are typically fixed, which cannot accommodate the volatile risk of the frequency insecurity. Nowadays, most generators adopt digital electro-hydraulic governors, and **they can change PFC droop gains according to the secure operation requirement of the power system** [20]. Thus, this paper proposes a novel strategy to change the droop gains of PFC resources hourly and optimize them at the day-ahead UC stage.

Apart from ensuring frequency security by PFC, power systems also need SFC to guarantee the frequency quality. SFC requires a certain reserve capacity to counteract the power fluctuation, while excessive reserve capacity increases the operational cost. Therefore, a proper setting of SFC reserve capacity is also essential to operate the power system safely and economically [21], [22], [23], [24].

Traditional methods of the SFC reserve capacity calculation are usually based on operational experience [25], [26], [27], [28]. The significant improvements in power system informatization and fast developments in data science enable more scientific approaches to determine the SFC reserve capacity.

Historical operation data contain the relationship among power fluctuation, SFC reserve capacity, and frequency control performance, which can be utilized to determine the SFC reserve capacity. Yang et al. proposed to evaluate the SFC reserve capacity adequacy by calculating the conditional probability of reaching the control performance standard under the available SFC reserve capacity [24]. The fluctuation intensities of loads and renewable generations are time-varying, making the requirement of SFC reserve capacity also time-dependent. Nevertheless, this method does not utilize the information of future power fluctuations. Zhang et al. built a multiple linear regression model, which reflects the relationship among the power fluctuation, SFC reserve capacity, and frequency control performance, to calculate the SFC reserve requirement [23]. However, the regression-based method cannot reflect and manage the risk of frequency control limit violation, which is less flexible than the probability-based method. Moreover, the existing methods may face challenges when the historical data are insufficient or inaccurate, because the established relationship may be unfaithful. **And this may result in errors when calculating the SFC reserve capacity requirement.** This situation often happens

while more and more wind power or solar power plants integrate to the grid.

Most of the existing literature only considers the post-fault frequency security constraints or mainly focuses on the frequency control reserve capacity in the UC problem, while both of these two factors affect the UC optimization. Zhang et al. made a preliminary study considering the two factors simultaneously [29], where the primary frequency response is simplified as a constant ramp function of time, and the SFC reserve capacity is determined without properly considering the frequency control performance.

To compensate for the insufficiency of the existing research, this paper proposes a UC model considering the frequency security constraints and frequency control capacity requirements. The major contributions are summarized as follows:

1) A novel extreme learning machine-based FNC linearization method is proposed in this paper, whose fitting accuracy is higher than the existing methods.
2) The droop gains of frequency regulation resources are optimized in the UC model to provide the PFC service adaptively considering different risks of frequency insecurity.
3) A novel SFC reserve capacity calculation method is proposed based on the Copula theory and distributionally robust optimization technique.

The remainder of the paper is organized as follows. Section II introduces the basic idea of this paper. The frequency security constraints are developed in Section III. Section IV introduces the data-driven SFC reserve capacity calculation method. The proposed UC model is given in Section V. Section VI presents the numerical experiments. Section VII concludes this paper.

II. Research Motivations

The power balance in power systems is typically achieved by three coordinated processes: the day-ahead unit commitment, intra-day economic dispatch, and real-time frequency control. The power fluctuations in traditional power systems are mild because they mainly come from the load demands, leading to a relatively low difficulty for system frequency control. The high penetration of renewable generations has increased the difficulty of power system frequency control. Thus, the frequency control requirements should be more carefully considered during the power system scheduling process.

A. Necessity of Considering Frequency Security Constraints in Unit Commitment

UC determines the on-off statuses of TGs, and thus directly decides the system inertia and available PFC resources. Moreover, the most significant power disturbance in power system operation is generally the dropping of the generator with the highest power output, which also depends on the UC results. These three factors significantly impact the system frequency deviation after the equipment failure, so the operational plan obtained from UC has prominent influences on the post-fault system frequency security. Therefore, it is essential to consider frequency security constraints in UC optimization.

B. Merit of Optimizing PFC Droop Gains in UC

In addition to the large-scale integration of centralized renewable power generations, electric vehicles and distributed generations on the demand side are also proliferating. The increasing converter-interfaced resources have led to significant heterogeneities in power system generation and load resources. Besides, their power injections/consumptions are strongly random and fluctuant, making the frequency response parameters highly variational and significantly influencing the frequency security constraints. For example, a higher risk of the FNC violation exists when the system inertia level is lower than its average value.

The droop gain decides the power adjustment quantity from PFC, which substantially affects the quasi-steady-state frequency and frequency nadir. Nevertheless, the static and fixed droop gains may face challenges in dealing with the dynamic-changing frequency response parameters. This study proposes to combat the dynamic-changing control system with the dynamic-changing PFC droop gain. Specifically, **droop gains of PFC resources are set hourly and optimized in the day-ahead UC stage**.

The benefits of this strategy lie in two aspects: first, the variable droop gain allows a PFC resource to make different control efforts in different operational risks, which helps to improve the frequency security; second, the variable droop gain can decrease the number of generators that are forced being started to guarantee the frequency security constraints, thereby saves the power system operational cost. The PFC droop gains are coupled with the ON/OFF statuses of generators, so droop gains should be optimized in the UC stage.

C. Necessity of Considering Frequency Control Capacity Requirements in Unit Commitment

Power systems need certain frequency control reserve capacities to counteract the power fluctuations. Online TGs provide the majority of frequency control reserve. The allocation of frequency control reserve capacities and the dispatch of power generation resources are two closely coupled problems, which should be jointly optimized in the UC stage to improve the economic efficiency of power system operation.

The calculation of PFC and SFC reserve requirements is essential for operating the power system safely and economically. Based on the droop gain of a PFC resource and the maximum allowable frequency deviation of the system, the maximum power support that needs to be provided by this resource during PFC can be calculated, and PFC reserve capacity can be determined. Nevertheless, SFC reserve requirement is mainly determined by operational experience, which may be unsafe and uneconomical under the largely variable operating conditions caused by the high proportion of renewable generations. Therefore, the determination of the SFC reserve requirement is also an important issue.

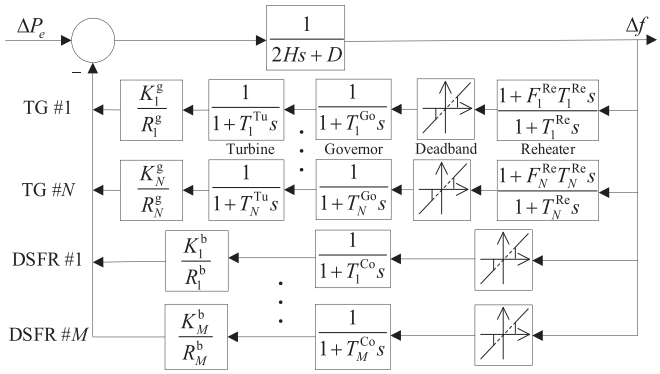

Fig. 1. Centralized frequency response model.

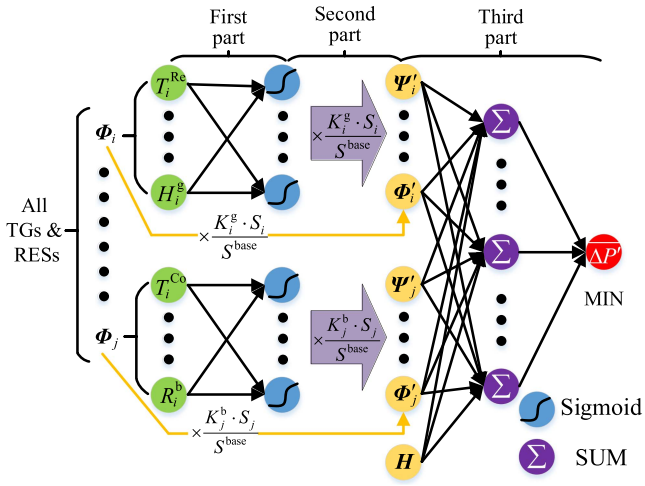

Fig. 2. Extreme learning machine-based prediction model of FNCPD.

III. Frequency Security Constraints and Primary Frequency Control

A. Frequency Security Constraints

Fig. 1 illustrates a centralized frequency response model comprised of TGs and converter-interfaced DSFRs, such as battery energy storage systems. It is assumed that the renewable generation resource neither provides inertia response nor participates in frequency control in this paper. For a TG without a reheater, F^{Re} and T^{Re} are set as 0.

To guarantee frequency security, the power system operator requires some post-fault dynamic frequency metrics must stay within their limitations. These frequency security metrics are introduced as follows.

1) RoCoF: In the first few seconds following the large power disturbance, the frequency droop is only arrested by the inertia response from the online synchronous units. To avoid triggering the RoCoF relay, the RoCoF in a measurement window should be limited. The RoCoF constraint can be guaranteed by restricting the highest value of RoCoF, which happens at the very instant of the outage.

$$\left|\dot{f}_{\max}\right| = \frac{|\Delta P|}{2H \cdot S^{\mathrm{base}}} \le RoCoF_{\max} \tag{1}$$

2) Quasi-Steady-State Frequency Deviation: A few seconds after the power disturbance, PFC will arrest the frequency decay and then recover it to the quasi-steady-state. The quasi-steady-state frequency deviation and its security constraint are expressed as follows

$$\Delta f^{\mathrm{QSS}} = \frac{|\Delta P|}{S^{\mathrm{base}} \cdot \left(D + R^{\mathrm{g}}_{\sum} + R^{\mathrm{b}}_{\sum}\right)} \le \Delta f^{\mathrm{QSS}}_{\max}, \tag{2}$$

where $R^{\mathrm{g}}_{\sum}$ and $R^{\mathrm{b}}_{\sum}$ are the integrated droop factors of TGs and DSFRs, as

$$R^{\mathrm{g}}_{\sum} = \frac{1}{S^{\mathrm{base}}} \cdot \sum_{i \in \mathcal{I}} \left(S^{\mathrm{g}}_i \cdot \frac{K^{\mathrm{g}}_i}{R^{\mathrm{g}}_i}\right), R^{\mathrm{b}}_{\sum} = \frac{1}{S^{\mathrm{base}}} \cdot \sum_{j \in \mathcal{J}} \left(S^{\mathrm{b}}_j \cdot \frac{K^{\mathrm{b}}_j}{R^{\mathrm{b}}_j}\right). \tag{3}$$

3) Frequency Nadir: The frequency response model shown in Fig. 1 is a high order model, making the frequency nadir formulation very complex. To simplify the model, authors in [13], [30] omit the regulator deadband, the governor and turbine blocks of TG, and assume that $T^{\mathrm{Re}} = T \gg T^{\mathrm{Co}} \approx 0$. Then, the FNC after a stepwise disturbance $\Delta P_e(s) = -\Delta P/s$ is formulated as (4). The detailed derivations can be found in [13], [30].

$$\left|\Delta f^{\mathrm{nadir}}\right| = \frac{|\Delta P|}{S^{\mathrm{base}} \cdot \left(D + R^{\mathrm{g}}_{\sum} + R^{\mathrm{b}}_{\sum}\right)} \times \left(1 + \sqrt{\frac{T\left(R^{\mathrm{g}}_{\sum} - F\right)}{2H}} e^{-\zeta \omega_n t_m}\right) \le \Delta f^{\mathrm{Nadir}}_{\max} \tag{4}$$

The above FNC is highly nonlinear because the parameters $R^{\mathrm{g}}_{\sum}$, $R^{\mathrm{b}}_{\sum}$, F, H, ζ, ω_n, and t_m depend on the ON/OFF statuses of generators and the droop gains of the PFC resources, making the power system scheduling model a nonlinear programming problem that is computationally intractable.

B. Extreme Learning Machine-Based FNCPD Forecast Model

As shown in (4), the frequency nadir is proportional to the power disturbance, implicating that the frequency deviation limitation $\Delta f^{\mathrm{Nadir}}_{\max}$ corresponds to a maximum tolerable disturbance power $\overline{\Delta P}$ of the power system. Furthermore, the FNC can be ensured by restricting the TGs' power outputs below the FNCPD. However, FNCPD changes with the operational state of the power system (decision variables of the UC problem). In this paper, a new extreme learning machine-based model is designed for the FNCPD forecast task, as shown in Fig. 2. The proposed network constitutes a **linear mapping** from the decision variables to the FNCPD, so it can be used for FNC linearization.

In the first part of the network, the original parameters of each TG/RES are transformed by a linear function and input to the sigmoid activation function ϑ, and the output of the sigmoid

activation function is the new synthetic parameter, as

$$\Psi_{i/j}^{\eta}=\vartheta\left(\boldsymbol{a}_{\eta}^{\mathrm{g/b}}\cdot\boldsymbol{\Phi}_{i/j}+b_{\eta}^{\mathrm{g/b}}\right),\forall i\in\mathcal{I},j\in\mathcal{J},1\leq\eta\leq\mathcal{N}, \tag{5}$$

where $\boldsymbol{\Phi}_i \triangleq \left\{T_i^{\mathrm{Re}},T_i^{\mathrm{Go}},T_i^{\mathrm{Tu}},F_i^{\mathrm{Re}},R_i^{\mathrm{g}},H_i^{\mathrm{g}}\right\}$, $\boldsymbol{\Phi}_j \triangleq \left\{T_j^{\mathrm{Co}},R_j^{\mathrm{b}}\right\}$. Although the sigmoid activation function in this part of network is nonlinear, the input variables of this part do not contain the decision variables of the power system scheduling model. Thus, this part of network will not make the proposed forecast model become nonlinear to the decision variables.

In the second part of the network, the new characteristic parameters along with the original parameters are multiplied by the mechanical/electrical power gain $K_{i/j}^{\mathrm{g/b}}$ and the normalized capacity of TG/RES, as

$$\boldsymbol{\Psi}_i'=K_i^{\mathrm{g}}\cdot\frac{S_i}{S^{\mathrm{base}}}\cdot\boldsymbol{\Psi}_i,\boldsymbol{\Phi}_i'=K_i^{\mathrm{g}}\cdot\frac{S_i}{S^{\mathrm{base}}}\cdot\boldsymbol{\Phi}_i,\forall i\in\mathcal{I}, \tag{6-a}$$

$$\boldsymbol{\Psi}_j'=K_j^{\mathrm{b}}\cdot\frac{P_j}{S^{\mathrm{base}}}\cdot\boldsymbol{\Psi}_j,\boldsymbol{\Phi}_j'=K_j^{\mathrm{b}}\cdot\frac{P_j}{S^{\mathrm{base}}}\cdot\boldsymbol{\Phi}_j,\forall j\in\mathcal{J} \tag{6-b}$$

The total system inertia is calculated in the second part of network, as

$$H=\frac{1}{S^{\mathrm{base}}}\cdot\left[\sum_{i\in\mathcal{I}}\left(H_i^g\cdot S_i\cdot x_i^{\mathrm{g}}\right)+\sum_{e\in\varepsilon}\left(S_e\cdot H_e\right)\right], \tag{7}$$

where e and ε are the index and the set of other machines providing inertia.

In the third part of the network, the piecewise linearization technique is utilized to fitting the frequency security margin:

$$\overline{\Delta P'}=\min_{1\leq l\leq\mathcal{L}}\left(\boldsymbol{c}_l\cdot\left[\boldsymbol{\Psi}',\boldsymbol{\Phi}',H\right]^{\top}+h_l\right), \tag{8}$$

where l and L are the index and number of segments of the piecewise linear function, respectively, $\boldsymbol{c}_l/h_l$ is the coefficient vector/scalar of the first-degree/constant item of the piecewise linear function, $\boldsymbol{\Psi}'$ is a vector composed of every TG's $\boldsymbol{\Psi}'_i$ and every RES's $\boldsymbol{\Psi}'_j$, $\boldsymbol{\Phi}'$ is similar to $\boldsymbol{\Psi}'$.

By assuming that the damping coefficient D is in direct proportion to the load power, and choosing the load power as the power base value S_t^{base}, the normalized damping coefficient D is a constant and can be omitted from the model.

C. Training of the FNCPD Forecast Model

Most machine learning models are trained by the gradient descent and backpropagation algorithms, and only the local optimal solution of the network parameters can be guaranteed. The proposed FNCPD prediction model is trained by solving the mixed-integer linear programming problem below, so the global optimal solution can be found.

$$\min_{\overline{\Delta P'_k},\boldsymbol{c}_l,h_l,\tilde{y}_{l,k}}\quad\sum_{k=1}^{N_{\mathrm{S}}}\left(\overline{\Delta P_k}-\overline{\Delta P'_k}\right)$$

$$\text{s.t.}\quad\overline{\Delta P_k}-\overline{\Delta P'_k}\geq 0,\forall k,$$

$$0\leq\left(\boldsymbol{c}_l\cdot\left[\boldsymbol{\Psi}',\boldsymbol{\Phi}',H\right]_k^{\top}+h_l\right)-\overline{\Delta P'_k}\leq\tilde{y}_{l,k}\cdot\mathcal{M},\forall k,l,$$

$$\sum_{1\leq l\leq\mathcal{L}}\tilde{y}_{l,k}=\mathcal{L}-1,\forall k,$$

$$\tilde{y}_{l,k}\in\{0,1\},\forall k,l. \tag{9}$$

Here, k and N_{S} are the index and the number of training samples, $\overline{\Delta P_k}$ and $\overline{\Delta P'_k}$ are the actual and predicted frequency security margins of the k^{th} data sample, respectively. The first constraint is added because a negative prediction error of the FNCPD will result in an insecure case being misidentified as a secure case. The second to fourth constraints represent the proposed prediction model, which is transformed from (8) by utilizing the big-M method.$\mathcal{M}$ is the auxiliary constant in the big-M method, whose values is set as 1 in this paper. $\tilde{y}_{l,k}$ is the auxiliary variable used in the big-M method.

The whole fitting process of the proposed method is proceeded by solving an optimization problem. Therefore, it can avoid the superposition and amplification of the fitting error compared with the multistage approximation method.

D. Primary Frequency Control Constraints

This study proposes to combat the dynamic-changing control system with the variable PFC droop gain. When optimizing droop gains of the PFC resources, the following constraints should be added to the UC model:

$$x_i^{\mathrm{PFC}}\cdot\underline{M}_i\leq K_{i,t}^{\mathrm{g/b}}\leq x_i^{\mathrm{PFC}}\cdot\overline{M}_i,\qquad\forall i\in\{\mathcal{I},\mathcal{J}\}, \tag{10}$$

$$x_i^{\mathrm{PFC}}\leq x_i^{\mathrm{UC}},\forall i\in\mathcal{I}, \tag{11}$$

$$\boldsymbol{c}_\ell\cdot\left[\boldsymbol{\Psi'}_{\{\mathcal{I},\mathcal{J}\}\backslash i},\boldsymbol{\Phi'}_{\{\mathcal{I},\mathcal{J}\}\backslash i},H_{\mathcal{I}\backslash i}\right]^{\top}+h_\ell\geq\frac{P_{i,t}}{S_t^{\mathrm{base}}},\ \forall i\in\mathcal{I},\ell,t \tag{12}$$

$$\frac{P_{i,t}}{2\cdot\left(H_t\cdot S_t^{\mathrm{base}}-H_{i,t}\cdot x_{i,t}^{\mathrm{UC}}\cdot P_i^{\max}\right)}\leq RoCoF^{\max},\ \forall i\in\mathcal{I},t \tag{13}$$

$$\frac{P_{i,t}}{\sum_{j\in\{\mathcal{I},\mathcal{J}\}\backslash i}K_{j,t}^{\mathrm{g/b}}\cdot P_j^{\max}\Big/R_j+S_t^{\mathrm{base}}\cdot D}\leq\Delta f_{\max}^{\mathrm{QSS}},\qquad\forall i\in\mathcal{I},t \tag{14}$$

$$r_{i,t}^{\mathrm{PFC}+/-}\geq\frac{K_{i,t}^{\mathrm{g/b}}}{R_i}\cdot P_i^{\max}\cdot\Delta f_{\max}^{\mathrm{Nadir}},\qquad\forall i\in\{\mathcal{I},\mathcal{J}\},\forall t \tag{15}$$

Equation (10) restricts the droop gain ranges of PFC resources. Eq. (11) indicates that a TG in OFF state cannot participate in the PFC. FNC is guaranteed by (12), where $\{\mathcal{I},\mathcal{J}\}\backslash i$ means that the generator i is out of service. Constraint (12) requires that after tripping any single generator, the FNCPD of the power system composed of other online generators and DSFRs should be larger than the power output of the failed generator constraint. (13) and (14) are the RoCoF and steady frequency deviation constraints, respectively, and they are developed based on (1) and (2). Eq. (15) guarantees that the PFC

reserve capacity is sufficient even when the frequency deviation reaches its upper limit. In constraints (12)–(14), S_t^{base} changes for every UC optimization time interval because the load is chosen as the base power.

Remark 1: According to the theorem in [31], the droop gain $K > 0$ guarantees that the control system can converge to a unique stable equilibrium. In other words, the PFC droop gains obtained from our research will not damage the small-signal stability of the system.

IV. SFC Reserve Capacity Determination

Properly setting the SFC reserve capacity is also essential to operate the power system safely and economically. This section introduces the proposed SFC reserve capacity calculation method, whose objective is to choose a minimum SFC reserve capacity enough for the AGC system to satisfy the power balancing control performance standard.

A. Power Balancing Control Performance Standard

The North American Electric Reliability Corporation (NERC) has published several standards to measure frequency control performance [32]. Considering that the historical data are taken from an actual control area adopting A_1/A_2 standard, A_1/A_2 standard is used as the control performance standard in this paper. The proposed method also applies to control areas adopting the CPS standard. The definition of A_1 is the times of the area control error (ACE) crossing zero within a stipulated timespan, and A_2 is the average ACE over this period, as

$$A_2 = \frac{1}{\Gamma}\sum_{\tau=1}^{\Gamma} ACE_\tau, \tag{16}$$

where Γ is the timespan, ACE_τ is the τ^{th} ACE in this period. A_1 only qualitatively reflects whether the ACE crosses zero, while A_2 quantitively shows the control performance. Therefore, the quantification of the SFC reserve requirement is based on A_2 in this research.

B. Criteria for Adequacy of SFC Reserve Capacity

In power systems, the power variations from load power and renewable generations mainly cause frequency fluctuations. In this paper, the changes of load power and renewable generations from the start to the end of a time interval are used to describe their variations. The power variation intensity is time-varying, so it should be forecasted before calculating the SFC reserve capacity requirement of a time interval. In this research, the extreme learning machine-based interval prediction method [33] is utilized to forecast the ranges of the power variations. The forecasted power fluctuation intervals are denoted as $[\underline{\boldsymbol{d}}, \overline{\boldsymbol{d}}]$, where $\underline{\boldsymbol{d}}$ is composed of the lower limits of load, wind, and solar power variations and $\overline{\boldsymbol{d}}$ is composed of the corresponding upper limits.

Given the forecasted power fluctuation intervals $[\underline{\boldsymbol{d}}, \overline{\boldsymbol{d}}]$, the SFC reserve capacity r should be selected to guarantee that the conditional probability of compliance of frequency control standard, under the predicted power fluctuations and chosen SFC reserve capacity, is larger than the preset confidence coefficient α, as

$$\mathbb{P}\left(|A_2| \le A_2^* | \underline{\boldsymbol{d}} \le \boldsymbol{d} \le \overline{\boldsymbol{d}}, r - \Delta r \le r^{\text{SFC}} \le r + \Delta r\right) \ge \alpha \tag{17}$$

where A_2^* is the threshold value specified in the control performance standard, $\boldsymbol{d}$ is the set composed of the load, wind, and solar power variations, Δr is used to form the range of SFC reserve capacity, r^{SFC} is the historical SFC reserve capacity.

C. Copula-Based Joint Distribution Model

The high-dimensional probability in (17) cannot be accurately calculated through statistics on historical data. To solve this problem, the conditional probability model (17) is built through the Copula theory. Because errors are inevitable when constructing the probability model, distributionally robust optimization techniques are used to calculate the SFC reserve requirement based on the built probability model.

Considering that the upward SFC reserve requirement is not related to the downward SFC reserve capacity and vice versa, the joint distribution of $A_2, \boldsymbol{d}, r^{\text{SFC}+}$ and that of $A_2, \boldsymbol{d}, r^{\text{SFC}-}$ are built separately. To avoid repetitiveness, we use r^{SFC} to denote $r^{\text{SFC}+}$ or $r^{\text{SFC}-}$ in the following descriptions.

Copula theory is an effective tool to build multivariate distribution [34]. It transforms the construction of joint cumulative distribution into modeling the marginal distributions and fitting the Copula function. By utilizing the Copula theory, the joint cumulative distribution function (CDF) of A_2, $\boldsymbol{d}$, and r^{Sec} is shown as

$$\begin{aligned}&\mathcal{F}_{A_2,\boldsymbol{d},r^{\text{SFC}}}\left(A_2, \boldsymbol{d}, r^{\text{SFC}}\right)\\ &= \mathcal{C}_{A_2,\boldsymbol{d},r^{\text{SFC}}}\left(\mathcal{F}_{A_2}\left(A_2\right), \ldots, \mathcal{F}_{d_{\text{S}}}\left(d_{\text{S}}\right), \ldots, \mathcal{F}_{r^{\text{SFC}}}\left(r^{\text{SFC}}\right)\right)\end{aligned} \tag{18}$$

where $\mathcal{F}$ is the cumulative distribution function, $\mathcal{C}$ is the Copula function, $\mathcal{F}_{A_2}(A_2)$, $\mathcal{F}_{d_{\text{S}}}(d_{\text{S}})$, and $\mathcal{F}_{r^{\text{SFC}}}(r^{\text{SFC}})$ are the marginal CDFs of A_2, d_{S}, and r^{SFC}, respectively. The joint probability density function (PDF) $f_{A_2,\boldsymbol{d},r^{\text{SFC}}}$ of A_2, $\boldsymbol{d}$, and r^{SFC} is the derivative of the joint CDF $\mathcal{F}_{A_2,\boldsymbol{d},r^{\text{SFC}}}$ on A_2, $\boldsymbol{d}$, and r^{SFC}, as

$$\begin{aligned}f_{A_2,\boldsymbol{d},r^{\text{SFC}}}\left(A_2, \boldsymbol{d}, r^{\text{SFC}}\right) &= \frac{\partial \mathcal{F}_{A_2,\boldsymbol{d},r^{\text{SFC}}}\left(A_2, \boldsymbol{d}, r^{\text{SFC}}\right)}{\partial A_2 \partial \boldsymbol{d} \partial r^{\text{SFC}}}\\ &= \varsigma_{A_2,\boldsymbol{d},r^{\text{SFC}}}\left(\mathcal{F}_{A_2}\left(A_2\right), \ldots, \mathcal{F}_{d_{\text{S}}}\left(d_{\text{S}}\right), \ldots, \mathcal{F}_{r^{Sec}}\left(r^{\text{SFC}}\right)\right)\\ &\quad \cdot f_{A_2}(A_2) \cdot \prod_{d \in \boldsymbol{d}} f_d(d) \cdot f_{r^{\text{SFC}}}(r^{\text{SFC}}).\end{aligned} \tag{19}$$

The conditional PDF of A_2 under $\boldsymbol{d}$ and r^{SFC} can be calculated through dividing the joint PDF $f_{A_2,\boldsymbol{d},r^{\text{SFC}}}(A_2, \boldsymbol{d}, r^{\text{SFC}})$ by the joint PDF $f_{\boldsymbol{d},r^{\text{SFC}}}(\boldsymbol{d}, r^{\text{SFC}})$, as

$$\begin{aligned}f_{A_2|\boldsymbol{d},r^{\text{SFC}}}\left(A_2|\boldsymbol{d}, r^{\text{SFC}}\right) &= \frac{f_{A_2,\boldsymbol{d},r^{\text{SFC}}}\left(A_2,\boldsymbol{d},r^{\text{SFC}}\right)}{f_{\boldsymbol{d},r^{Sec}}(\boldsymbol{d},r^{\text{SFC}})}\\ &= \frac{\varsigma_{A_2,\boldsymbol{d},r^{\text{SFC}}}\left(\mathcal{F}_{A_2}(A_2),\ldots,\mathcal{F}_{d_{\text{S}}}(d_{\text{S}}),\ldots,\mathcal{F}_{r^{Sec}}\left(r^{\text{SFC}}\right)\right)\cdot f_{A_2}(A_2)}{\varsigma_{\boldsymbol{d},r^{\text{SFC}}}\left(\mathcal{F}_{d_{\text{L}}}(d_{\text{L}}),\ldots,\mathcal{F}_{r^{Sec}}(r^{\text{SFC}})\right)}\end{aligned} \tag{20}$$

The joint PDF $f_{\boldsymbol{d},r^{\text{SFC}}}(\boldsymbol{d}, r^{\text{SFC}})$ can be built in a similar way as (18), (19).

There are many different functions that can be used as the Copula function C to build the joint distribution. This study first chooses the most commonly used functions, including Gaussian Copula, Student-t Copula, Clayton Copula, Gumbel Copula, and Frank Copula, to build the joint distribution (18). Then, the Bayesian information criterion (*BIC*) [35] is utilized to assess the fitting performances of different models, as

$$BIC = -2\ln\left(\tilde{l}\right) + q * \ln(\mathcal{X}), \tag{21}$$

where q is the number of parameters that need to be fitted in the Copula function, $\tilde{l}$ represents the value of the maximum likelihood function [36], and $\mathcal{X}$ indicates the number of data points used in building the model.

D. Distributionally Robust Chance Constraint

The historical data may be insufficient or inaccurate when newly integrated renewables exist, based on which the estimated probability model is unfaithful. Furthermore, this may lead the calculated SFC reserve capacity requirement to be inappropriate. To handle the possible errors in the probability model, chance constraint (17) is reformulated as a distributionally robust chance constraint, which requires that the chance constraint is satisfied for all the PDFs within the ambiguity set constructed from the samples [37], as

$$\min_{\mathbb{Q}\in\widehat{\mathcal{P}}} \mathbb{P}^{\mathbb{Q}}\left(|A_2| \le A_2^* | \underline{\boldsymbol{d}} \le \boldsymbol{d} \le \overline{\boldsymbol{d}}, r-\Delta r \le r^{\mathrm{SFC}} \le r+\Delta r\right) \ge \alpha. \tag{22}$$

In this research, the ambiguity set $\widehat{\mathcal{P}}$ is built based on the Wasserstein metric. The distance between distributions $\mathbb{Q}_1$ and $\mathbb{Q}_2$ defined by the Wasserstein metric is formulated as:

$$\mathcal{D}_{\mathrm{W}}\left(\mathbb{Q}_1, \mathbb{Q}_2\right) = \sup_{f\in\mathbb{L}} \left\{ \int_{\Xi} f(\xi)\mathbb{Q}_1(\mathrm{d}\xi) - \int_{\Xi} f(\xi)\mathbb{Q}_2(\mathrm{d}\xi) \right\}, \tag{23}$$

where ξ is the stochastic variable belonging to the value space $\Xi \triangleq \{\xi \in \mathbb{R} : \mathcal{B}\xi \le \mathcal{H}\}$, $\mathbb{L}$ denotes the spaces of all Lipschitz functions with $|f(\xi) - f(\xi')| \le |\xi - \xi'|$ for all $\xi_1, \xi_2 \in \Xi$. The ambiguity set is defined as a Wasserstein ball that and can be expressed as

$$\widehat{\mathcal{P}} \triangleq \left\{ \mathbb{Q} : \mathcal{D}_{\mathbb{W}}\left(\widehat{\mathbb{P}}, \mathbb{Q}\right) \le \varepsilon \right\}, \tag{24}$$

where $\widehat{\mathbb{P}}$ is the empirical distribution constructed from the data set composed of historical data and sample data taken from (20) conditioned on the forecasted power variation intervals and the SFC reserve capacity range $[r-\Delta r, r+\Delta r]$, and ε is the radius of the Wasserstein ball.

Conditional value at risk (CVaR) is a risk measure that quantifies the expected loss over the part of distribution beyond the confidence level [38]. The distributionally robust chance constraint (22) is transformed by utilizing the CVaR approximation [39], as

$$\max_{\mathbb{Q}\in\widehat{\mathcal{P}}} \mathbb{E}^{\mathbb{Q}}\left[\max\left(\frac{A_2 - A_2^* - \delta^0}{1-\alpha}, \frac{-A_2 - A_2^* - \delta^0}{1-\alpha}, 0\right) + \delta^0\right] \le 0. \tag{25}$$

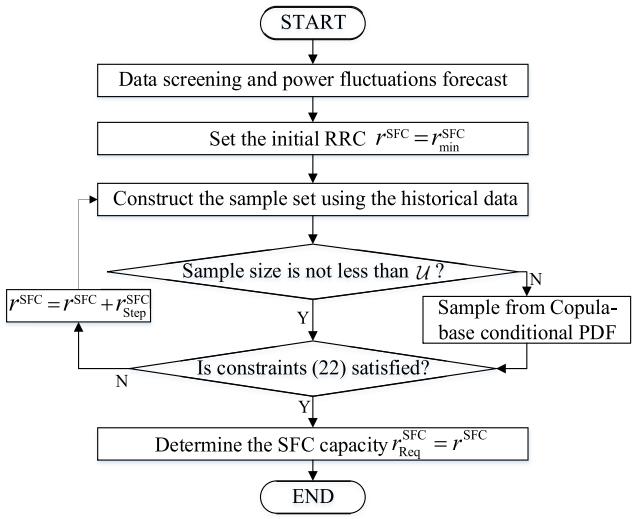

Fig. 3. The flowchart of SFC reserve capacity calculation.

Then, (25) can be reformulated to a set of constraints according to [37, Corollary 5.1], as

$$\begin{cases} \lambda\varepsilon + \frac{1}{\mathcal{U}}\sum_{\mu=1}^{\mathcal{U}} \sigma_\mu \le 0, \\ \frac{A_{2,\mu} - A_2^* + \alpha\delta^0}{1-\alpha} + \gamma_\mu^1 \cdot (\mathcal{H} - \mathcal{B}\cdot A_{2,\mu}) \le \sigma_\mu, \forall\mu, \\ \frac{-A_{2,\mu} - A_2^* + \alpha\delta^0}{1-\alpha} + \gamma_\mu^2 \cdot (\mathcal{H} - \mathcal{B}\cdot A_{2,\mu}) \le \sigma_\mu, \forall\mu, \\ \delta^0 + \gamma_\mu^3 \cdot (\mathcal{H} - \mathcal{B}\cdot A_{2,\mu}) \le \sigma_\mu, \forall\mu, \\ \left\| \mathcal{A}^\top\gamma_\mu^1 - \frac{1}{1-\alpha}, \mathcal{A}^\top\gamma_\mu^2 + \frac{1}{1-\alpha}, \mathcal{A}^\top\gamma_\mu^3 \right\|_\infty \le \lambda, \forall\mu, \\ \gamma_\mu^1, \gamma_\mu^2, \gamma_\mu^3 \ge 0, \forall\mu, \end{cases} \tag{26}$$

where λ, σ_μ, γ_μ^1, γ_μ^2, γ_μ^3 are auxiliary variables, μ and $\mathcal{U}$ are the index and the total number of the data samples, respectively. $\mathcal{H}$ and $\mathcal{B}$ are used to restrict the value space of A_2, as $\Xi \triangleq \{A_2 \in \mathbb{R} : \mathcal{B}\xi \le \mathcal{H}\}$.

Constraints in (26) can be used to check whether an SFC reserve capacity r is sufficient to fulfill the frequency control standard. The flowchart of the SFC reserve requirement calculation is shown in Fig. 3. The upward and downward SFC reserve capacity requirements should be calculated separately.

V. Modified Unit Commitment Model

The UC optimization model considering the frequency security constraints and frequency control capacity requirements is developed in this section. The frequency security constraints and the constraints on PFC droop gain have been introduced in Section III. The SFC reserve capacity are determined according to Section IV, as shown in Fig. 4.

A. Objective Function

The objective function of the UC model is to minimize the total operational cost, including the generation and start-up costs of TGs, as well as reserve costs of all frequency regulation

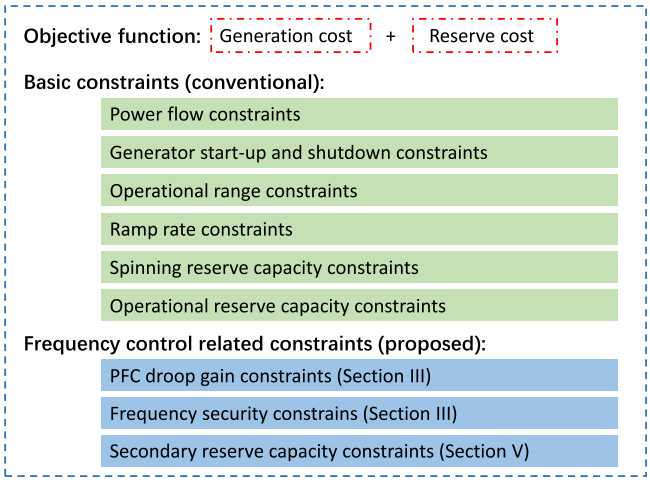

Fig. 4. Framework of the proposed UC model.

resources.

$$\text{Min.} \sum_{t\in\mathcal{T}} \left\{ \sum_{i\in\mathcal{I}} \left(C_i^{\text{SU}} y_{i,t} + C_{i,t}^{\text{Gen}}\right) + \sum_{i\in\{\mathcal{I},\mathcal{J}\}} C_i^{\text{Spin}} \left(r_{i,t}^{\text{Spin}+} + r_{i,t}^{\text{Spin}-}\right) \right\} \tag{27}$$

The generation cost of TG *i* can be formulated as follows:

$$C_{i,t}^{\text{Gen}} = \max_{k\le K} \left(\phi_{i,k}^{\text{g}} \cdot P_{i,t}^{\text{g}} + \varphi_{i,k}^{\text{g}}\right), \quad \forall i \in \mathcal{I}, t. \tag{28}$$

B. Constraints

The operational constraints in the UC model are presented as follows:

1) Power Flow Constraints:

$$\sum_{i\in\mathcal{I}_n} P_{i,t}^{\text{g}} + \sum_{i\in\mathcal{J}_n} P_{i,t}^{\text{b}} - L_{n,t} = \sum_{m:(n,m)\in\Im} B_{n,m}\left(\theta_{n,t} - \theta_{m,t}\right), \forall n, t \tag{29}$$

$$B_{n,m}\left(\theta_{n,t} - \theta_{m,t}\right) \le W_{n,m}, \quad \forall (n,m) \in \Im, t \tag{30}$$

Equation (29) is the DC power flow constraint, where $m : (n,m) \in \Im$ denotes the buses connected with bus *n*, and $\Im$ is the set of all branches. It is assumed that the base operational points of DSFRs are known and cannot be scheduled. Equation (30) is the line capacity constraint. The base power in the power flow constraints is fixed.

2) Generator Start-Up and Shutdown Constraints:

$$y_{i,t} \ge x_{i,t}^{\text{g}} - x_{i,t-1}^{\text{g}}, \qquad \forall i \in \mathcal{I}, t \tag{31}$$

$$z_{i,t} \ge x_{i,t-1}^{\text{g}} - x_{i,t}^{\text{g}}, \qquad \forall i \in \mathcal{I}, t \tag{32}$$

$$\sum_{\tau=t-T_i^{\text{ON}}}^{t-1} x_{i,\tau}^{\text{g}} \ge z_{i,t} T_i^{\text{ON}}, \quad \forall i \in \mathcal{I}, t \tag{33}$$

$$\sum_{\tau=t-T_i^{\text{OFF}}}^{t-1} \left(1 - x_{i,\tau}^{\text{g}}\right) \ge y_{i,t} T_i^{\text{OFF}}, \qquad \forall i \in \mathcal{I}, t \tag{34}$$

Equations (31) and (32) are the start-up and shutdown logical constraints for TGs. Equations (33) and (34) are the minimum online and offline time constraints of TGs.

3) Operational Range Constraints:

$$P_{i,t}^{\text{g/b}} + r_{i,t}^{\text{Spin}+} \le P_i^{\max} x_{i,t}^{\text{g}}, \quad \forall i \in \{\mathcal{I},\mathcal{J}\}, t \tag{35}$$

$$P_{i,t}^{\text{g/b}} - r_{i,t}^{\text{Spin}-} \ge P_i^{\min} x_{i,t}^{\text{g}}, \quad \forall i \in \{\mathcal{I},\mathcal{J}\}, t \tag{36}$$

Equations (35), (36) restrict that the base operational points of the TGs and DSFRs plus/minus the upward/downward spinning reserve capacities are within their ranges.

4) Ramp Rate Constraints:

$$P_{i,t} - P_{i,t-1} \le x_{i,t} V_i + y_{i,t} P_i^{\min}, \quad \forall i \in \mathcal{I}, t \tag{37}$$

$$P_{i,t-1} - P_{i,t} \le x_{i,t-1} V_i + z_{i,t} P_i^{\min}, \forall i \in \mathcal{I}, t \tag{38}$$

Equations (37) and (38) are the ramp rate constraints between the adjacent dispatch points of the TG, where the start-up and shutdown states are considered. The ramp rate constraints for DSFR are not considered because their ramp rates are fast.

5) Reserve Capacity Constraints:

$$r_{i,t}^{\text{Spin}+/-} \ge r_{i,t}^{\text{PFC}+/-} + r_{i,t}^{\text{SFC}+/-} + r_{i,t}^{\text{Op}+/-}, \forall i \in \{\mathcal{I},\mathcal{J}\}, t \tag{39}$$

$$\sum_{i\in\{\mathcal{I},\mathcal{J}\}} r_{i,t}^{\text{SFC}+/-} \ge r_{\text{Req},t}^{\text{SFC}+/-}, \qquad \forall t \tag{40}$$

$$\sum_{i\in\{\mathcal{I},\mathcal{J}\}} r_{i,t}^{\text{Op}+/-} \ge r_{\text{Req},t}^{\text{Op}+/-}, \qquad \forall t \tag{41}$$

For each resource, the spinning reserve capacity should be larger than the sum of PFC, SFC, and operation reserve capacities, as (39). The sum of upward/downward SFC reserve capacity provided by all resources should be larger than the upward/downward SFC reserve capacity requirement calculated by utilizing the method proposed in Section IV. The system operation reserve capacity requirement also needs be satisfied, as (41). The system operation reserve requirement is taken as a certain percentage of the system total load power.

6) Primary Frequency Control Constraints: The PFC constraints (10)–(15) should also be included in the UC optimization model.

Remark 2: The forecast errors of the renewable generations are not considered in this UC model because it is not the focus of this study. In fact, there are tremendous methods to handle this issue, and they can be easily introduced into this UC model [40], [41], [42], [43].

VI. Case Study

A. Case Settings

The IEEE 118-bus system is used for the case study. We modified it by connecting six wind farms to buses 1, 44, 68, 17,

TABLE I
GENERATOR PARAMETERS

Generator (# bus)	12	26	89	59,61	65,66	10,69, 80	25,49, 100	31,46, 87	54,103, 111
Reserve cost ($/MWh)	7.2	9	9.6	7.8	9.6	9	7.8	6	7.2
Start-up cost ($)	120	400	800	240	500	600	300	80	100
Ramp rate (MW/min)	2	7	13	4	8	10	5	1.5	1.8
Min. ON/OFF time (h)	2	6	8	4	8	6	4	2	2

TABLE II
DSFR CONVERTER PARAMETERS

DSFR (# bus)	19	34	49	62	75	77
Capacity (MW)	40	30	30	33	40	30
Time constant (s)	0.01	0.01	0.01	0.01	0.01	0.01
Reserve cost ($/MW)	4	4	4	5	5	5
Droop factor	0.15	0.15	0.15	0.15	0.15	0.15

76, 89 with installed capacities of 400 MW, 300 MW, 300 MW, 330 MW, 400 MW, 300 MW, and four photovoltaic plants to buses 18, 24, 32, 38 with installed capabilities of 400 MW, 400 MW, 330 MW, 300 MW, respectively. The generator parameters in the frequency response model are taken from [44], and other generator parameters are listed in Table I. The parameters of DSFRs are shown in Table II. The PFC droop gain range of each TG is from 0.5 to 1, and the droop gain range of each DSFR is from 0 to 2.

The proposed method needs historical data of AGC control performance, SFC reserve capacities, load power, and renewable generations. In this paper, the data from a practical power system in North China are used. The time resolutions of load power and renewable generations are minutely, and the resolutions of historical SFC reserve capacity and AGC control performance A_2 data are fifteen-minutely. All the historical data are scaled down for the simulations. The historical data from 2016 to 2018 with a total of 821 days are randomly split into training and test sets at a ratio of 6 to 4. The training set is used to train the extreme learning machine-based forecast model and build the Copula-based joint distribution model.

B. Frequency Nadir Constraint Approximation Accuracy

The training of the FNC linearization method requires the ON/OFF status of the generators, the droop gains of the PFC resources, and the corresponding FNCPD. To obtain the training data, we perform UC simulations over a whole year on the test system by utilizing the model proposed in Section IV-B-3 of [11]. The above-mentioned historical data of load power and renewable generations are scaled down to fit the test system and then used as the input for the UC simulation. Considering that the droop gain K^{b} is tunable when DSFRs participating in the primary frequency control, K^{b} is generated from the uniform distribution U(02) for each hour. To make a rigorous statistical evaluation of the performance of the proposed method, some noises are added to the data set obtained from the UC simulation to generate extra ten data sets.

After obtaining the data of ON/OFF status of the generators and the droop gains of the PFC resources, the detailed system frequency response model (shown in Fig. 1) is used to simulate the system FNCPD for each data sample. The resolution of the frequency data is 0.02 second. The simulation is carried out using Simulink in the MATLAB environment. This frequency response model contains the governor deadband, so the influence of the governor deadband on the proposed method can be tested.

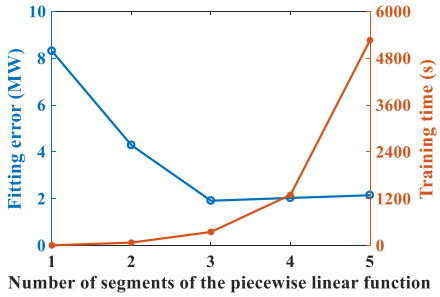

Fig. 5. Training time and fitting error under different numbers of segments of the piecewise linear function.

TABLE III
TAGS OF CLASSIFICATION RESULTS

		Predicted result	
		Violation	No violation
Real state	Violation	True positive (TP)	False positive (FP)
	No violation	False negative (FN)	True negative (TN)

Several advanced FNC linearization methods are compared in this subsection to show the superiority of the proposed FNC linearization method. The values of the hyper-parameters in different methods are given as below.

Proposed method: The neuron number in the hidden layer of the extreme learning machine is 10 for each TG/RES. The number of segments for the piecewise linear function is 3, i.e., $L = 3$ in Fig. 2.

Multistage approximation method [14]: The number of segments for the piecewise linear function is 40.

Optimal decision tree-based method [15]: The depth of the optimal decision tree is set as 2.

Deep neural network-based method [16]: The number of the hidden layer is set as 1, and the neuron number is 256. The values of these hyper-parameters are taken from the original.

Remark 3: The hyperparameter L is determined through sensitivity analysis. The proposed method is trained and tested under different values of L. The training time and fitting error are plotted in Fig. 5. The fitting error reduces rapidly before $L = 3$, and the training time increases significantly after $L = 3$. The classifier performance evaluation indices are defined as follows:

An FNC can be viewed as a classifier judging whether the frequency nadir caused by a large power disturbance will exceed the limitation. Thus, we use classifier performance indices to compare different FNC linearization methods. Since each test sample can be tagged according to its real and predicted states, as shown in Table III, the classifier performance indices are defined as follows:

$$\text{Accuracy} = \frac{N_{\mathrm{TP}} + N_{\mathrm{TN}}}{N_{\mathrm{TOT}}}, \text{Recall} = \frac{N_{\mathrm{TP}}}{N_{\mathrm{TP}} + N_{\mathrm{FN}}},$$

TABLE IV
CLASSIFIER PERFORMANCE INDICES OF DIFFERENT FNC LINEARIZATION METHOD

Index	Proposed	Multistage approximation	Optimal decision tree	Deep neural network
Accuracy	**99.91 %**	97.94 %	99.47 %	69.34 %
Recall	**100 %**	100 %	99.37 %	100 %
Precision	**99.87 %**	98.46 %	99.83 %	68.58 %
F1 score	**99.93 %**	98.46 %	99.60 %	81.35 %

$$\text{Precision} = \frac{N_{\text{TP}}}{N_{\text{TP}} + N_{\text{FP}}}, \text{F1} = \frac{2 \cdot \text{Precision} \cdot \text{Recall}}{\text{Precision} + \text{Recall}},$$

where N_{TP}, N_{FP}, N_{FN}, N_{TN} denote the numbers of samples with TP, FP, FN, and TN tags, respectively. N_{TOT} is the total number of the test samples. The classifier performance indices of different FNC linearization methods are given Table IV, which is based on the test results on eleven different test sets.

From Table IV, it can be found that all indices of proposed method are the **highest** compared with other methods. The recall rate of the proposed method is 100%, proving that the FNCs obtained by the proposed method is a safe approximation of the original FNC. In other words, no insecure case will be identified as the secure case by utilizing the proposed approximation method. The proposed method, multistage approximation method, and the optimal decision tree-based method train the FNC approximation model by solving linear problems, which can guarantee that the calculated model parameters are optimal. The DNN based method train the network through gradient descent and backpropagation, which is hard to obtain the optimal parameters. This explains why the performance of the DNN based FNC approximation method is poorer than other three methods.

C. Comparison With the Traditional UC Model

The proposed UC model is first compared with the traditional UC Model. The algorithm is executed on a 24-hour horizon, and the optimization time interval is 15 minutes. Each test day is simulated independently. In the traditional UC model, the PFC droop gain is fixed, the frequency security constraints are not considered, and the SFC reserve capacity is the same as the historical data. After the UC results of different models are obtained, we simulated the PFC after the failure of the largest generator in each hour of the test days by utilizing the Simulink in MATLAB environment. Due to the traditional UC model does not consider the frequency security constraint, at least one frequency security constraint is violated for a probability of 15.37% in the test hours. The violation ratio of the frequency security constraint for the proposed model is 0, revealing the safety of the proposed modeling method for the frequency security constraint. Fig. 6 plots the frequency curves after the failure of the largest generator in the same test hour for the proposed UC model and the traditional one. The frequency security constraints are violated under the traditional UC model.

Table V gives the comparison results of the proposed and the traditional UC models. The generation cost of the traditional model is smaller than that of the proposed model because the traditional model does not consider the frequency security constraints. Nevertheless, the PFC reserve cost of the traditional model is larger than that of the proposed model because the proposed model adopts the variable PFC droop gain that helps lower the PFC reserve cost. The comparison on the SFC reserve costs illustrates that the proposed SFC reserve capacity quantification method can lower the SFC reserve cost.

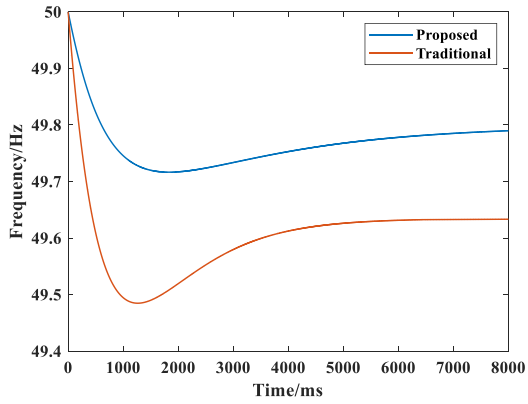

Fig. 6. Frequency curves after the failure of the largest generator.

TABLE V
COMPARISONS OF THE OPERATIONAL COSTS AND INFEASIBLE CASE RATIO OF THE PROPOSED AND TRADITIONAL UC MODELS

Model	Proposed	Traditional
Generation cost (10^5 \$)	9.69	9.64
PFC reserve cost (10^5 \$)	1.02	1.15
SFC reserve cost (10^5 \$)	0.16	0.25
Operation reserve cost (10^5 \$)	0.26	0.28
Operational cost (10^5 \$)	11.13	11.32
Frequency security constraint violation ratio (%)	0	15.37

After the UC results of different models are obtained, we simulated the PFC after the failure of the largest generator in each hour of the test days by utilizing the Simulink in MATLAB environment. Due to the traditional UC model does not consider the frequency security constraint, at least one frequency security constraint is violated for a probability of 15.37% in the test hours. The violation ratio of the frequency security constraint for the proposed model is 0, revealing the safety of the proposed modeling method for the frequency security constraint. Fig. 6 plots the frequency curves after the failure of the largest generator in the same test hour for the proposed UC model and the traditional one. The frequency security constraints are violated under the traditional UC model.

D. Comparison of Other UC Models

The proposed UC model is compared with the other six UC models to demonstrate its superiority. The model settings are given in Table VI.

1) Comparison of Operational Cost: The comparison results of different models are shown in Table VII. It can be found from Table VII that the operational cost of model A is the smallest. Fig. 7 plots the ratios of other models' operational costs to model

TABLE VI
STRATEGIES OF DIFFERENT MODELS

Model	PFC droop gain	FNC approximation	SFC reserve
A	Variable	Proposed	Proposed
B	Fixed	Proposed	Proposed
C	Variable	Proposed	Historical Data
D	Variable	Multistage approximation	Proposed
E	Variable	Optimal decision tree	Proposed
F	Variable	Deep neural network	Proposed

TABLE VII
COMPARISON OF THE OPERATIONAL COSTS AND INFEASIBLE CASE RATIO OF DIFFERENT MODELS

Model	A	B	C	D	E	F
Generation cost (10^5 \$)	9.69	9.71	9.69	9.70	9.70	9.70
PFC reserve cost (10^5 \$)	1.02	1.54	1.02	1.18	1.09	1.03
SFC reserve cost (10^5 \$)	0.16	0.16	0.25	0.16	0.16	0.16
Operation reserve cost (10^5 \$)	0.26	0.27	0.26	0.26	0.26	0.26
Operational cost (10^5 \$)	11.13	11.68	11.22	11.30	11.21	11.15
Infeasible case ratio (%)	1.83	5.81	2.14	5.20	1.84	2.45

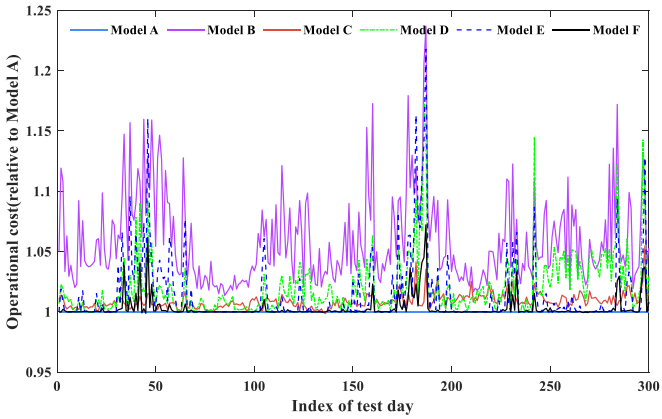

Fig. 7. Operational costs of different methods in the test set.

A's operational cost on each test days, it also illustrates that the operational cost of model A is smaller than those of the other two models on all test days. These results prove that the proposed UC model is more economically efficient. The operational cost of model B is the highest, which proves that the fixed PFC droop gain has the largest influence on the operational cost.

2) Analysis of the Infeasible Case Ratio: Some test cases are infeasible due to no operation plan satisfying all constraints. It can be found from Table VII that the ratio of the infeasible case of model A is smaller than that of model B. The variable PFC droop gain strategy increases the safe operational region of the power system operation, and some infeasible cases due to the violation of frequency security constraints become feasible after adopting the proposed strategy.

The infeasible case ratio of model A is smaller than those of model D to model F, which illustrates that the FNC linearization by the proposed method is less conservative than those built by the methods proposed in references [13], [15], [16].

3) Comparison of Primary Frequency Control Reserve Cost: PFC reserve costs of these six models are compared in Fig. 8. The PFC reserve cost of model A is smaller than that of model B, proving that the strategy of optimal PFC droop gain helps save the reserve cost.

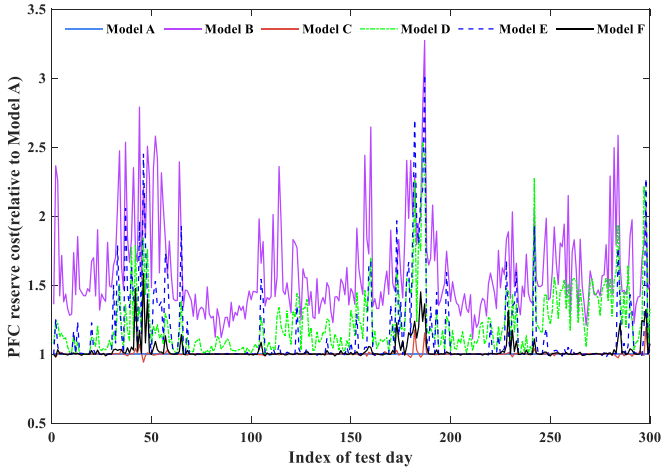

Fig. 8. Comparison on primary frequency control reserve costs of six models.

TABLE VIII
COMPARISON OF OPERATIONAL COSTS OF DIFFERENT MODELS

Method	Upward SFC capacity (MW)	Downward SFC capacity (MW)
Proposed	154.45	179.55
Historical	244.64	265.54

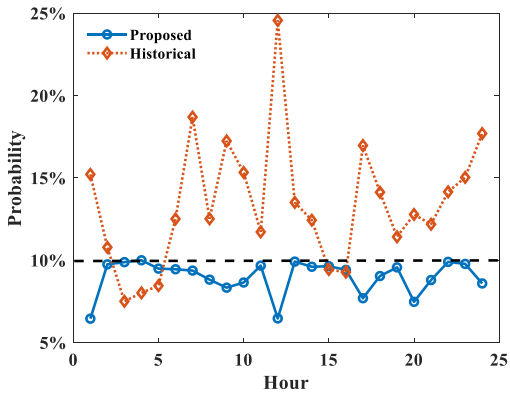

Fig. 9. Comparison on probability of $|A_2|$ exceeding the specified value.

The PFC reserve cost of model A is also lower than those of model D to model F, revealing that the FNC linearization method proposed in this paper is better than the method proposed in references [13], [15], [16].

4) SFC Reserve Requirement: As shown in Table VIII, in the whole test set, the average SFC reserve capacity requirements calculated by the proposed method are smaller than the average SFC capacities in the actual historical data.

Furthermore, we select the historical time intervals whose actual SFC reserve capacities are close to their calculated SFC reserve capacities to reflect the frequency control performance of the proposed method. The probability of $|A_2|$ exceeding the specified value (40 MW) is calculated on the selected data set and all historical data in the test set, as shown in Fig. 9. The probabilities under the proposed method are no larger than

TABLE IX
COMPARISON OF THE COMPUTATION TIME OF SIX MODELS

Model	A	B	C	D	E	F
Computation time (s)	42.37	110.37	129.48	102.11	141.31	238.12

the specified limitation (10%) in all hours. In comparison, the probabilities of historical data are higher than the limitation in many hours, which illustrates that the proposed method can improve the frequency control performance.

These results show that the SFC reserve requirement calculated by the proposed method is more appropriate than the actual SFC reserve capacity in the historical operation.

E. Computation Efficiency

This subsection tests the computation efficiencies of different methods. The experiments are conducted on a PC with an Intel i7-7700 CPU 3.6 GHz and 16 GB of memory. The GUROBI solver [45] is utilized to solve the MILP problem. The average computation times of the six models on all test days are calculated and shown in Table IX. It can be found that the computation time of model A is the smallest. The computation time of model F is the longest because it introduces a large number of integer variables in FNC linearization.

VII. CONCLUSION

This paper builds a UC model considering the frequency security constraints and frequency control reserve requirements. On the frequency security constraint, an extreme learning machine-based linearization method for frequency nadir constraint is presented. Then, a novel SFC reserve requirements calculation method is proposed by combining the Copula theory and distributionally robust optimization technique. Moreover, the variable PFC droop gain strategy is put forward to adopt for the volatile risks of frequency constraint violation. The simulation results conducted on the IEEE 118-bus system show that:

1) The proposed FNC linearization method provides a closer approximation to the original FNC, which helps to improve the system frequency security and lower the PFC reserve cost.
2) The optimal PFC droop gain strategy can reduce the reserve cost and increase the feasible region of the security-constrained UC problem compared with the fixed PFC droop gain setting adopted for the current operation.
3) The SFC reserve requirement calculated by the proposed method is more appropriate than the actual SFC reserve capacity in the historical operation, which helps to achieve better frequency control performance and to save the SFC reserve capacity.

In this research, the modeling of the DSFR is comparatively rough. In future works, specific models of diverse DSFRs will be utilized in the proposed UC model.

REFERENCES

[1] IRENA, "Global renewables outlook: Energy transformation 2050," Apr. 2020. [Online]. Available: https://www.irena.org/publications/2020/Apr/Global-Renewables-Outlook-2020

[2] F. Milano, F. Dörfler, G. Hug, D. J. Hill, and G. Verbič, "Foundations and challenges of low-inertia systems (invited paper)," in *Proc. Power Syst. Comput. Conf.*, 2018, pp. 1–25.

[3] L. Hao, J. Ji, D. Xie, H. Wang, W. Li, and P. Asaah, "Scenario-based unit commitment optimization for power system with large-scale wind power participating in primary frequency regulation," *J. Modern Power Syst. Clean Energy*, vol. 8, no. 6, pp. 1259–1267, Nov. 2020.

[4] Z. Chu, U. Markovic, G. Hug, and F. Teng, "Towards optimal system scheduling with synthetic inertia provision from wind turbines," *IEEE Trans. Power Syst.*, vol. 35, no. 5, pp. 4056–4066, Sep. 2020.

[5] X. Zhu, Z. Yu, and X. Liu, "Security constrained unit commitment with extreme wind scenarios," *J. Modern Power Syst. Clean Energy*, vol. 8, no. 3, pp. 464–472, May 2020.

[6] Y. Wen, W. Li, G. Huang, and X. Liu, "Frequency dynamics constrained unit commitment with battery energy storage," *IEEE Trans. Power Syst.*, vol. 31, no. 6, pp. 5115–5125, Nov. 2016.

[7] National Grid, "Future requirements for balancing services," 2016. [Online]. Available: https://www.nationalgrideso.com/document/88586/download

[8] Q. Shi, F. Li, and H. Cui, "Analytical method to aggregate multi-machine SFR model with applications in power system dynamic studies," *IEEE Trans. Power Syst.*, vol. 33, no. 6, pp. 6355–6367, Nov. 2018.

[9] I. Egido, F. Fernandez-Bernal, P. Centeno, and L. Rouco, "Maximum frequency deviation calculation in small isolated power systems," *IEEE Trans. Power Syst.*, vol. 24, no. 4, pp. 1731–1738, Nov. 2009.

[10] F. Teng, V. Trovato, and G. Strbac, "Stochastic scheduling with inertia-dependent fast frequency response requirements," *IEEE Trans. Power Syst.*, vol. 31, no. 2, pp. 1557–1566, Mar. 2016.

[11] H. Ahmadi and H. Ghasemi, "Security-constrained unit commitment with linearized system frequency limit constraints," *IEEE Trans. Power Syst.*, vol. 29, no. 4, pp. 1536–1545, Jul. 2014.

[12] M. Paturet, U. Markovic, S. Delikaraoglou, E. Vrettos, P. Aristidou, and G. Hug, "Stochastic unit commitment in low-inertia grids," *IEEE Trans. Power Syst.*, vol. 35, no. 5, pp. 3448–3458, Sep. 2020.

[13] Z. Zhang, E. Du, F. Teng, N. Zhang, and C. Kang, "Modeling frequency dynamics in unit commitment with a high share of renewable energy," *IEEE Trans. Power Syst.*, vol. 35, no. 6, pp. 4383–4395, Nov. 2020.

[14] Z. Zhang et al., "Modeling frequency response dynamics in power system scheduling," *Electric Power Syst. Res.*, vol. 189, 2020, Art. no. 106549.

[15] D. T. Lagos and N. D. Hatziargyriou, "Data-driven frequency dynamic unit commitment for island systems with high RES penetration," *IEEE Trans. Power Syst.*, vol. 36, no. 5, pp. 4699–4711, Sep. 2021.

[16] Y. Zhang et al., "Encoding frequency constraints in preventive unit commitment using deep learning with region-of-interest active sampling," *IEEE Trans. Power Syst.*, vol. 37, no. 3, pp. 1942–1955, May 2022.

[17] Y. Zhang, C. Chen, G. Liu, T. Hong, and F. Qiu, "Approximating trajectory constraints with machine learning–microgrid islanding with frequency constraints," *IEEE Trans. Power Syst.*, vol. 36, no. 2, pp. 1239–1249, Mar. 2021.

[18] H. Huang and F. Li, "Sensitivity analysis of load-damping characteristic in power system frequency regulation," *IEEE Trans. Power Syst.*, vol. 28, no. 2, pp. 1324–1335, May 2013.

[19] A. Ulbig, T. S. Borsche, and G. Andersson, "Impact of low rotational inertia on power system stability and operation," *IFAC Proc. Volumes*, vol. 47, no. 3, pp. 7290–7297, 2014.

[20] A. Dixon, *Modern Aspects of Power System Frequency Stability and Control*. New York, NY, USA: Academic, 2019.

[21] F. Zhang, Z. Hu, X. Xie, J. Zhang, and Y. Song, "Assessment of the effectiveness of energy storage resources in the frequency regulation of a single-area power system," *IEEE Trans. Power Syst.*, vol. 32, no. 5, pp. 3373–3380, Sep. 2017.

[22] S. Pulendran and J. E. Tate, "Capacity scheduling of energy storage and conventional generation for frequency regulation based on CPS1," *IEEE Trans. Power Syst.*, vol. 35, no. 1, pp. 405–414, Jan. 2020, doi: 10.1109/tpwrs.2019.2924019.

[23] G. Zhang and J. D. McCalley, "Estimation of regulation reserve requirement based on control performance standard," *IEEE Trans. Power Syst.*, vol. 33, no. 2, pp. 1173–1183, Mar. 2018.

[24] Y.-R. Yang, C.-C. Shen, C.-C. Wu, and C.-N. Lu, "Control performance based dynamic regulation reserve allocation for renewable integrations," *IEEE Trans. Sustain. Energy*, vol. 10, no. 3, pp. 1271–1279, Jul. 2019.
[25] PJM Interconnection, LLC, "PJM manual 12: Balancing operations," Oct. 2019. [Online]. Available: https://www.pjm.com/~/media/documents/manuals/m12.ashx
[26] New York, NY, USA ISO, Inc, "NYISO ancillary services manual," Oct. 2019. [Online]. Available: https://www.nyiso.com/documents/20142/2923301/ancserv.pdf
[27] ISO New England, Inc, "ISO new england manual for the regulation market," Oct. 2019. [Online]. Available: https://www.iso-ne.com/static-assets/documents/2014/09/m_11_market_operations_revision_47_10_06_13.doc
[28] California ISO Corporation, "Business practice manual for market operations," 2020. [Online]. Available: https://bpmcm.caiso.com/BPM%20Document%20Library/Market%20Operations/BPM_for_Market%20Operations_V54_redline.pdf
[29] G. Zhang, E. Ela, and Q. Wang, "Market scheduling and pricing for primary and secondary frequency reserve," *IEEE Trans. Power Syst.*, vol. 34, no. 4, pp. 2914–2924, Jul. 2019.
[30] U. Markovic, Z. Chu, P. Aristidou, and G. Hug, "LQR-based adaptive virtual synchronous machine for power systems with high inverter penetration," *IEEE Trans. Sustain. Energy*, vol. 10, no. 3, pp. 1501–1512, Jul. 2019.
[31] W. Cui, Y. Jiang, and B. Zhang, "Reinforcement learning for optimal primary frequency control: A lyapunov approach," *IEEE Trans. Power Syst.*, vol. 38, no. 2, pp. 1676–1688, Mar. 2023.
[32] North American Electric Reliability Corporation, "BAL-001-2–Real power balancing control performance standard background document," 2013. [Online]. Available: https://www.nerc.com/pa/Stand/Project%202010141%20%20Phase%201%20of%20Balancing%20Authority%20Re/BAL-001-2_Background_Document_Clean-20130301.pdf
[33] C. Wan, J. Wang, J. Lin, Y. Song, and Z. Y. Dong, "Nonparametric prediction intervals of wind power via linear programming," *IEEE Trans. Power Syst.*, vol. 33, no. 1, pp. 1074–1076, Jan. 2018.
[34] E. Bouyé et al., "Copulas for finance-A reading guide and some applications," Financial Econometrics Research Centre, City University Business School, London, Available SSRN 1032533, 2000.
[35] D. Posada and T. R. Buckley, "Model selection and model averaging in phylogenetics: Advantages of akaike information criterion and bayesian approaches over likelihood ratio tests," *Systematic Biol.*, vol. 53, no. 5, pp. 793–808, 2004.
[36] R. J. Rossi, *Mathematical Statistics: An Introduction to Likelihood Based Inference*. Hoboken, NJ, USA: Wiley, 2018.
[37] P. Mohajerin Esfahani and D. Kuhn, "Data-driven distributionally robust optimization using the wasserstein metric: Performance guarantees and tractable reformulations," *Math. Prog.*, vol. 171, no. 1–2, pp. 115–166, 2017.
[38] J. Kisiala, *Conditional Value-at-Risk: Theory and Applications*. Edinburgh, U.K.: Univ. Edinburgh, 2015.
[39] A. R. Hota, A. Cherukuri, and J. Lygeros, "Data-driven chance constrained optimization under wasserstein ambiguity sets," in *Proc. Amer. Control Conf.*, 2019, pp. 1501–1506.
[40] H. Quan, D. Srinivasan, and A. Khosravi, "Incorporating wind power forecast uncertainties into stochastic unit commitment using neural network-based prediction intervals," *IEEE Trans. Neural Netw. Learn. Syst.*, vol. 26, no. 9, pp. 2123–2135, Sep. 2015.
[41] H. Pandžić, Y. Dvorkin, T. Qiu, Y. Wang, and D. S. Kirschen, "Toward cost-efficient and reliable unit commitment under uncertainty," *IEEE Trans. Power Syst.*, vol. 31, no. 2, pp. 970–982, Mar. 2016.
[42] P. Xiong, P. Jirutitijaroen, and C. Singh, "A distributionally robust optimization model for unit commitment considering uncertain wind power generation," *IEEE Trans. Power Syst.*, vol. 32, no. 1, pp. 39–49, Jan. 2017.
[43] Y. Teng, Q. Hui, Y. Li, O. Leng, and Z. Chen, "Availability estimation of wind power forecasting and optimization of day-ahead unit commitment," *J. Modern Power Syst. Clean Energy*, vol. 7, no. 6, pp. 1675–1683, Nov. 2019.
[44] "KIOS center for intellegent systems & networks, University of Cyprus," IEEE 118-bus modified test system, Nov. 2018. [Online]. Available: http://www.kios.ucy.ac.cy/testsystems/index.php/dynamicieee-test-systems/ieee--bus-modified-test-system118AD
[45] L. Gurobi Optimization, "Gurobi optimizer reference manual," 2021. [Online]. Available: http://www.gurobi.com

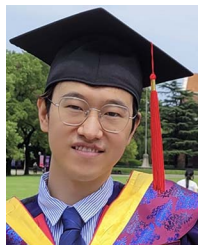

Likai Liu received the Ph.D. degree in electrical engineering, from Tsinghua University, Beijing, China, in 2022.

He is currently with JD.com as an Algorithm Engineer.

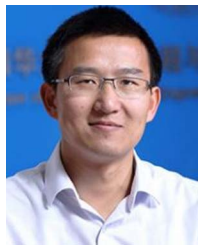

Zechun Hu (Senior Member, IEEE) received the B.S. and Ph.D. degrees in electrical engineering from Xi'an Jiao Tong University, Xi'an, China, in 2000 and 2006, respectively.

He was with Shanghai Jiao Tong University, Shanghai, China, and also with the University of Bath, Bath, U.K., as a Research Officer from 2009 to 2010. In 2010, he joined the Department of Electrical Engineering, Tsinghua University, Beijing, China, where he is currently an Associate Professor. His research interests include optimal planning and operation of power systems, electric vehicles, and energy storage systems.

Yilin Wen (Student Member, IEEE) received the B.S. degree in electrical engineering in 2020 from Tsinghua University, Beijing, China, where he is currently working toward the Ph.D. degree in electrical engineering.

His research interests include demand response, integrated transmission and distribution systems, and control and optimization in power systems.

Yuxin Ma (Student Member, IEEE) received the B.S. degree in electrical engineering in 2021 from Tsinghua University, Beijing, China, where she is currently working toward the Ph.D. degree in electrical engineering.

Her research interests include optimal operation and control of energy storage systems and power systems.